Asian Journal of Pharmaceutical Sciences 20 (2025) 100990

Available online at www.sciencedirect.com

ScienceDirect

journal homepage: www.elsevier.com/locate/AJPS

Research Article

Biomimetic nanoparticles co-deliver hirudin and lumbrukinase to ameliorate thrombus and inflammation for atherosclerosis therapy

Mengying Cheng[a], *Tianxiang Yue*[a], *Hong Wang*[a], *Lai Jiang*[a], *Qiaoling Huang*[b,*], *Fanzhu Li*[a,*]

[a] *Zhejiang Chinese Medical University, School of Pharmaceutical Sciences, Hangzhou, 310053, China*
[b] *Zhejiang Chinese medical university, Hangzhou Third People's Hospital, Hangzhou 310009, China*

ARTICLE INFO

Article history:
Received 18 May 2024
Revised 19 August 2024
Accepted 21 August 2024
Available online 2 November 2024

Keywords:
Atherosclerosis
Hirudin
Lumbrukinase
Biomimetic nanoparticle
Thrombolysis
Anti-inflammatory

ABSTRACT

Atherosclerosis (AS) is a progressive inflammatory disease, and thrombosis most likely leads to cardiovascular morbidity and mortality globally. Thrombolytic drugs alone cannot completely prevent thrombotic events, and treatments targeting thrombosis also need to regulate the inflammatory process. Based on the dynamic pathological development of AS, biomimetic thrombus-targeted nanoparticles HMTL@PM were prepared. Hirudin and lumbrukinase, effective substances of traditional Chinese medicine, were self-assembled under the action of tannic acid and Mn^{2+}. HMTL@PM dissociated in the weakly acidic microenvironment of atherosclerosis and exhibited excellent therapeutic effects, including alleviating inflammation, dissolving thrombus, anticoagulation, and promoting cholesterol efflux. HMTL@PM effectively regulated the progression of AS and provided a new perspective for the development of drug delivery systems for AS therapy, which holds important research significance for reducing the mortality of cardiovascular and cerebrovascular diseases.

1. Introduction

Atherosclerosis (AS), the major cause leading to high mortality from cardiovascular disease, is a persistent inflammatory disease with complex pathophysiology that progresses dynamically marked by infiltration of inflammatory cells and lipid deposition forming atherosclerotic plaques [1,2]. The initiation, occurrence, development and thrombus formation in atherosclerosis are all influenced by inflammation. In the early stage of AS, vascular endothelial injury causes the infiltrated macrophages to engulf the oxidized low-density lipoprotein (ox-LDL) and form foam cells, accelerating plaque formation and calcification [3,4]. In the progressive stage,

* Corresponding authors.
E-mail addresses: hql6512@163.com (Q. Huang), lifanzhu@zcmu.edu.cn (F. Li).
Peer review under responsibility of Shenyang Pharmaceutical University.

https://doi.org/10.1016/j.ajps.2024.100990

foam cells accumulate to form atherosclerotic plaques, vulnerable plaques are prone to rupture due to inflammation, hemorheology and other factors, activating the coagulation system, and platelet aggregation forms thrombi [5]. Persistent and occlusive thrombosis in the late stage leads to vascular stenosis, causing ischemic injury, which may give rise to clinical complications including myocardial infarction, as well as angina and stroke [6]. Therefore, removing thrombi and improving inflammation become the first choice for the treatment of atherosclerosis.

Platelets and the coagulation cascade are effective targets for anti-thrombotic therapy, but the use of thrombolytic drugs alone cannot completely prevent thrombotic events [7]. It indicates that there are still other mechanisms, such as inflammation, that have not been fully addressed, leading to therapeutic gaps [8]. Growing evidence points to the necessity for the thrombosis-targeting medications to inflammation-regulation, which adds to their positive benefits [9–11]. On the other hand, anti-inflammatory therapy can also decrease thrombotic instances. Thrombosis is closely related to inflammation, which promotes thrombosis by damaging the vascular endothelium, activating platelets and the clotting system, and increasing white blood cell involvement. Anti-inflammatory therapy can reduce endothelial damage, inhibit platelet and coagulation system activity, and reduce overall inflammation levels, thus effectively preventing and controlling thrombosis [12–14]. Traditional Chinese medicine (TCM) exhibits advantages in atherosclerosis treatment with multiple mechanistic approaches and fewer adverse reactions. The combination therapy of "Leech-Pheretima" has been proven to have excellent efficacy against AS. Hirudin (HV), as a natural thrombin-specific inhibitor, can irreversibly bind to thrombin to form tight non-covalent complexes, inhibiting the coagulation of fibrinogen and the action of thrombin on platelets, exhibiting efficient inhibition of platelet aggregation and thrombus formation, with broad prospects for application in cardiovascular diseases prevention and treatment [15–18]. Lumbrukinase (LK), extracted from the TCM pheretima, is a complex protein of fibrinolytic enzyme, which reduces the expression of vascular endothelial cell calcium-binding protein (VE-cadherin) by regulating the NF-κB pathway, inhibiting fibrinogen activation, reducing the infiltration of inflammatory macrophages, thus alleviating inflammation [19–22]. Additionally, LK can directly degrade fibrinogen in the blood, activate plasminogen to plasmin, further accelerating thrombus dissolution.

Due to the specificity of AS treatment, drugs need to meet the requirements of long circulation and precise targeting. Inspired by biological systems in nature, biomimetic drug delivery technologies have drawn a lot of interest lately [23–25]. This technology typically mimics natural mechanisms to achieve targeted effects, accurately delivering drugs to target sites, with good biocompatibility and safety, enhancing the therapeutic effects of drugs [26]. Biomimetic drug delivery systems can be broadly categorized into cells modified with targeting ligands, nanocarriers coated with cell membranes, and whole cells. Inspired by the responsive aggregation of platelets at thrombus sites, platelet membrane biomimetic nanocarrier systems offer a new opportunity for targeted therapy of atherosclerosis. Platelet membranes possess good biocompatibility, exhibit a natural homing effect to thrombus, and show a tendency towards sites of vascular endothelial injury and secondary microthrombi [27–32]. They emit the signal of ”don’t eat me” in order to prevent phagocytose and clearance from the reticuloendothelial system, therefore promoting prolonged circulation throughout the body [33–35].

On account of its polyphenol structure, tannic acid is capable of self-assembling with mental ions to form a metal-phenol network (MPN) structure under coordination, which can then encapsulate drugs and achieve pH responsive release [36,37]. In the selection of metal ions, studies have demonstrated that certain metal ions are associated with an increased risk of developing atherosclerotic diseases. For instance, calcium ions have been shown to accelerate the calcification of plaque in lesion sites. While Mn^{2+} plays an important role in lipid metabolism and can affect the synthesis and metabolism of cholesterol and fatty acids. Mn^{2+} could maintain normal lipid metabolism, thereby reducing lipid deposition in artery walls. Additionally, manganese ions have the potential to serve as imaging agents in future studies [38].

Herein, this work designed a novel biomimetic thrombus-targeted nanoparticle. The biomimetic nanoparticles, encapsulated with platelet membranes containing HV and LK, were prepared to actively target atherosclerotic thrombus sites and effectively ameliorate thrombus and inflammation (Fig. 1). Tannic acid-mediated self-assembly imparted the nanoparticles with the ability to respond to dissociate in response to the weakly acidic environment of thrombus. HV inhibited thrombin activity to inhibit thrombus formation, and combined with lumbrukinase’s effects on dissolving thrombus and regulating inflammation, aimed to achieve the purpose of treating atherosclerosis. We believed that this biomimetic nanoparticle overcome the limitations of AS treatment, prolonged drug circulation in the blood, reduced toxic side effects, significantly improved efficacy, reduced drug frequency, achieved stable drug release, and ultimately achieved efficient, long-lasting and safe therapeutic effects.

2. Materials and methods

2.1. *Materials*

Recombinant HV, LK and LPS were obtained from Yuanye Bio-Technology Co., Ltd. (China). Tannic acid and $MnCl_2$ were sourced from Macklin Biochemical Technology Co., Ltd. (China). NaOH was provided by Aladdin Biochemical Technology Co., Ltd. (China). Mouse peripheral blood platelet separation solution kit was purchased from TBD Co., Ltd. (China). Kinase buffer (10×) was supplied by MesGen Biotechnology Co., Ltd. (China). Fibrinogen was acquired from Meilun Biotechnology Co., Ltd. (China). Thrombin, ox-LDL and total cholesterol (TC) content assay kit were obtained from Solarbio Science & Technology Co., Ltd. (China). ATP (100 mM, nuclease-free), PMSF, DAPI, BCA protein assay kit, coomassie blue staining kit, reactive oxygen species assay kit, cell counting kit-8, modified oil red O staining kit, and Kinase-

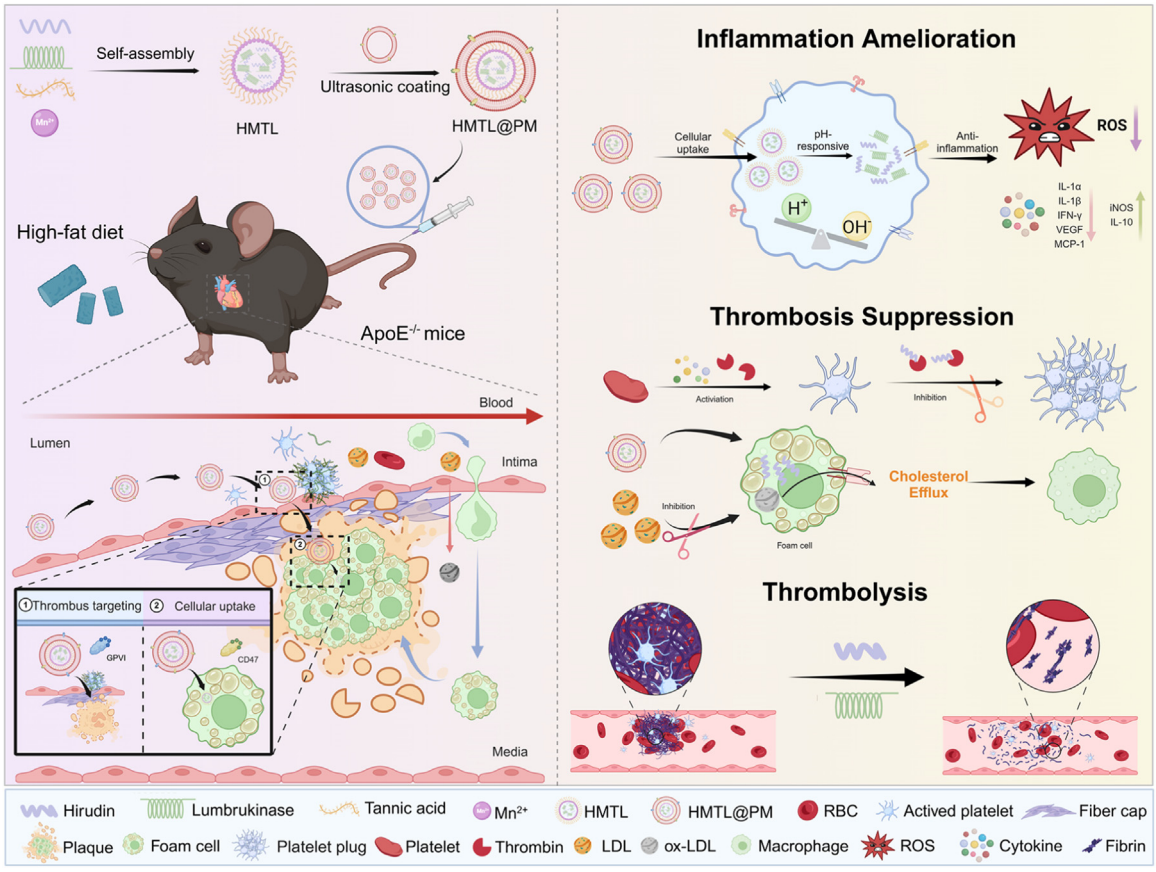

Fig. 1 – Schematic illustration of ameliorating thrombus and inflammation realized by HMTL@PM with plaque-targeting for atherosclerosis therapy.

Lumi^{TM} plus luminescent kinase assay kit were all sourced from Beyotime Biotechnology Co., Ltd. (China). Additionally, the Omni-Easy^{TM} One was utilized.

2.2. *Construction and characterization of HMTL@PM*

2.2.1. *Construction of HMTL@PM*

The HMTL@PM were fabricated by mixing HV, LK, $MnCl_2$ and TA in one pot through the TA-Mn^{2+} cross-linking action, and further coating platelet membranes on the surface through ultrasound (Fig. 2A). The detailed construction steps were as follows: 500 μl HV (1 mg/ml) and 500 μl LK (1 mg/ml) were dropped into the mixing solution of TA and $MnCl_2$ (mass ratio, TA: $MnCl_2$=2:1). The solution was ultrasonic for 1 min, and the NaOH (0.1 mol/l) was used to adjust the pH to 7.0 under intense agitation, then stirred at 25 °C overnight. The HMTL (nanoparticles that have not been coated with platelet membrane) were collected by centrifugation (13,000 r/min, 10 min), washed with ultrapure water for 3 times to remove unreacted raw materials, and stored at 4 °C after lyophilization. Whole blood was isolated from the orbital vein of BALB/c mice and anticoagulated using EDTA-K_2. The procedures were adapted from previously reported methods [39]. Purified platelets were obtained using the Mouse peripheral blood platelet separation solution kit. Added 200 μl PBS that contained 1 mM PMSF and carefully pipetted to resuspend the purified platelets. Then repeatedly frozen-thawed at −80 °C to isolate the platelet membranes from the platelets. Following centrifugation (4,000 g, 3 min, 4 °C) and washing with ultrapure water for 3 times, the purified platelet membranes (PM) were suspended in a mixture containing 1 mM PMSF and HMTL followed by sonication (mass ratio, platelet membrane protein: nanoparticle=1:1). The excess HMTL were removed by centrifugation (4,000 g, 3 min, 4 °C).

2.2.2. *Morphological characterization of HMTL@PM*

The morphology of HMTL, PM and HMTL@PM was visualized by TEM. Using Malvern Zetasizer, the hydrodynamic size and *zeta* potential of HMTL, PM and HMTL@PM were measured in PBS.

2.2.3. *Verification of the platelet membrane coating*

SDS-PAGE was applied to identify the protein content for the purpose to analyze the protein profiles of PM, HMTL and HMTL@PM. Initial voltage was set to 70 V firstly, which is adjusted to 85 V after the sample is electrophoresed to the separation gel. Using the Coomassie Blue Staining Kit, the whole gel was dyed on a shaker for 2 h, and the color was removed overnight with ultrapure water.

2.2.4. *Qualitative and quantitative methods to determine HV and LK*

To examine whether the tannic acid affects the measurement of total protein concentration, tannic acid solution with

concentration gradient was set up and determinated by BCA Protein Assay Kit. Similarly, the standard curve of TA-Mn^{2+} complex was established, the absorbance was the vertical coordinate and the protein concentration was the horizontal coordinate. In a range of 200–600 nm, the absorption spectra of HV, LK, TA and TA-Mn^{2+} complex solutions with a certain concentration were detected and compared. According to the characteristic absorption peak of TA-Mn^{2+}, the concentration gradients (0, 1, 2, 4, 6, 8, 10, 15, 20, 30 and 40 μg/ml) were set up to determine the absorbance at 350 nm and the standard curve was established. Precisely weighed 5 mg HMTL in 4 ml ultrapure water, then added 1 ml 5% HNO_3 and incubated for 24 h to promote the release of HV and LK. With the use of BCA Protein Assay Kit, total protein concentration of HMTL was calculated. The interference of tannic acid on the determination of total protein concentration could be eliminated by combining the established standard curve above. The content of LK was measured by Kinase-Lumi™ Plus Luminescent Kinase Assay Kit, and the standard curves of ATP and LK were established respectively. Finally, the content of HV was calculated.

2.2.5. *Assessment of loading capacity and encapsulation efficiency*

With the aim to choose the optimum drug reaction dosage, mixed different quantities of tannic acid with 1 mg HV and LK (mass ratio, polypeptide: polyphenol=1:1,1:2,1:3,1:4,1:5,1:6,1:7,1:8) to prepare HMTL. Measurement of particle size and *zeta* potential on the preparations with various proportions were performed. The drug loading efficiency (LE) of HV and LK were calculated according to the following formula, as well as encapsulation percentage (EN). The standard curve of Mn^{2+} was established by ICP-MS, and the loading efficiency of Mn^{2+} in HMTL@PM was determined.

$$LE(\%) = W_{\text{loaded drug}}/W_{\text{total nanoparticles}} \times 100\%$$

$$EN(\%) = W_{\text{loaded drug}}/W_{\text{total drug}} \times 100\%$$

2.2.6. *Release profiles* in vitro *of HV-LK loaded HMTL@PM*

Utilizing the dialysis method, the release profiles *in vitro* of HV-LK loaded HMTL@PM was investigated. Briefly, to simulate the drug release of HMTL@PM in the normal physiological environment, atherosclerotic plaque site and acid lysosomes of macrophages, varying pH values of PBS (7.4, 6.5 and 5.0) were used as the release medium. 10 mg HMTL was dispersed in PBS (pH 7.4) and packed into a dialysis bag (100 kDa). Immersed it in the corresponding simulated release media for different times (0.5, 1, 1.5, 2, 2.5, 3, 3.5, 4, 4.5, 5, 5.5, 6, 8, 12, 16, 20 and 24 h) at 37 °C while shaking continuously at 100 r/min. The same volume of prewarmed fresh PBS was quickly introduced after 1 ml external medium was removed at the designated time points. The contents of HV and LK were calculated respectively. Three duplicates of the experiment were conducted and the mean ± SD of the results was expressed.

2.2.7. *Biocompatibility assay*

For hemocompatibility assay, red blood cells (RBCs) were collected by centrifugation (1,500 r/min, 15 min) after whole blood had been anticoagulated with heparin sodium, followed by multiple PBS washes. Incubated HMTL@PM (50, 100, 150 and 200 μg/ml) with 2% RBCs suspension at 37 °C for 2 h After centrifugation (3,000 r/min, 5 min), the absorption at 540 nm was used to calculate the amount of hemoglobin present in the supernatant. ddH_2O was set as the positive group and negative control was saline group. According to the following formula, the hemolysis rate was determined.

$$\text{Hemolysis (\%)} = \frac{A_{\text{Sample}} - A_{\text{Negative}}}{A_{\text{Positive}} - A_{\text{Negative}}} \times 100\%$$

For the test of platelet aggregation, plasma-rich platelets (PRP) were collected from whole blood (1,500 r/min, 20 min). 100 μl PRP was mixed with PBS, HV (1 mg/ml), LK (1.25 mg/ml), HMTL@PM (2 mg/ml) and thrombin/$CaCl_2$ (1:5, v/v) in 96-well plate. Measured the absorbance of mixture at 650 nm in 1 h.

2.2.8. *Stability test*

The stability of platelet membrane proteins during 1-week storage was studied. Specifically, we extracted platelet membrane proteins on HMTL@PM at Day 1, 3, 5 and 7, then targeting function-related proteins GPVI and CD47 were selected for WB experiments. The storage stability of HMTL@PM was assessed by regularly monitoring its hydrodynamic size and zeta potential stored in ddH_2O at 4 °C for a month, every 3 d Additionally, the hydrodynamic size and zeta potential of HMTL@PM in RPMI 1640 (10% FBS) at 37 °C were examined to mimic a more actual blood-like environment. Moreover, the drug content in HMTL@PM solution during 1-week storage was measured to determine whether the HV or lumbrokinase was leaking.

2.3. In vitro *studies*

2.3.1. *Evaluation of cell toxicity*

The cytotoxicity of HMTL and HMTL@PM on RAW264.7 cells and HUVEC cells was investigated by assessing cell viability by Cell Counting Kit-8. Briefly, being seeded in 96-well plates (1×10^4 cells per well), cells were cultured overnight. HMTL or HMTL@PM were added to the sample group treating for 24 h (10, 20, 50, 75 and 100 μg/ml). The blank wells and the cells with blank medium were designated as the blank and the control group. Next, added 100 μl 10% CCK-8 solution into well, then left it in darkness for 2 h. The absorbance was determined at 450 nm, and calculated the cell viability based on the formula that follows:

$$\text{Cell viability (\%)} = \frac{OD_{\text{Sample}} - OD_{\text{Blank}}}{OD_{\text{Control}} - OD_{\text{Blank}}} \times 100\%$$

2.3.2. *Uptake of HMTL@PM by macrophage and HUVEC*

To simulate the pathological inflammatory microenvironment of atherosclerosis, a competitive assay was performed. RAW264.7 cells and HUVEC cells were divided into normal cells and inflammatory cells stimulated with 1 μg/ml LPS. Being seeded in a 25 mm confocal dish (1×10^5 cells

per dish), cells were cultured overnight. Then treated with ICG, ICG-labeled HMTL and ICG-labeled HMTL@PM for 4 h (ICG: 20 μg/ml). After that, washed with PBS, added 4% paraformaldehyde for fixation, and labeled with DAPI. The laser confocal microscopy (CLSM) was used to observed finally.

2.3.3. ROS-scavenging and anti-inflammatory capacity of HMTL@PM

The levels of ROS were detected by a reactive detection kit. RAW264.7 were seeded in a 25 mm confocal dish (5×10^5 cells per dish). After culturing overnight, treated with HMTL or HMTL@PM for 4 h, which was added 1 μg/ml LPS concurrently. Fresh medium was given to the normal group, while 1 μg/ml LPS was utilized to stimulate the model group. Next, 10 μM DCFH-DA probe was added, then incubated at 37 °C for 20 min. Washed with DMEM to remove the excess DCFH-DA and observed by CLSM.

Levels of cytokines including TNF-α, IL-1α, IL-1β, IL-10, MCP-1, IFN-γ, iNOS, VEGF and α-SMA were detected by ELISA kit. RAW264.7 were seeded in 6-well plates (5×10^5 cells per well), then cultured with 1 μg/ml LPS overnight. Then treated with HV, LK, HMTL and HMTL@PM for 24 h (ATU: 300 U/ml). The blank DMEM were set as the negative control, while DMEM with 1 μg/ml LPS was the positive control. Collected the cell culture medium and the supernatant was obtained by centrifugation (1,000 g, 20 min).

2.3.4. Binding affinity of HMTL@PM to activated platelets

Platelets were collected in a laser confocal dish and incubated with thrombin/$CaCl_2$ for 0.5 h, during which time platelet activation was induced. Then labelled platelets with CM-Dil. The samples were treated with ICG-HMTL or ICG-HMTL@PM for 1 h Next fixed with paraformaldehyde and observed under CLSM.

2.3.5. In vitro clot lysis test

The whole blood was mixed with an appropriate amount of thrombin (1 U/μl) and $CaCl_2$ (5 mg/ml), then stored at 4 °C for the clot formation. Following precise weighed (W_1), treated with HV, LK, HMTL (pH 7.4), HMTL@PM and HMTL (pH 5) for 2 h at 37 °C (ATU=5,000 U/ml). Then transferred the supernatant to measure the absorbance at 540 nm and 340 nm respectively. After removing the remaining supernatant, to cancel the thrombolysis, the clots were cleaned with PBS and weighed (W_2). Calculated the thrombolysis rate according to the formula:

$$\text{Thrombolysis rate (\%)} = \frac{W_1 - W_2}{W_1} \times 100\%$$

2.3.6. Anticoagulant effect assay

By centrifugation (1,500 r/min, 20 min), PRP were extracted from whole blood. 100 μl PRP was mixed with thrombin/$CaCl_2$ (1:5, v/v) in 96-well plate. Before fibrin clot formation, HV (1 mg/ml) and HMTL@PM (2 mg/ml) were added in PBS was set as the negative group and thrombin/$CaCl_2$ was the positive group. The absorbance of mixture was detected at 650 nm within 1 h.

2.3.7. Effects of hmtl@pm on foam cell formation

RAW264.7 and HUVEC were seeded in 6-well plate (RAW264.7: 2×10^5 cells per well, HUVEC: 1×10^5 cells per well). Treated with HV, LK, HMTL or HMTL@PM and co-incubated with 1 μg/ml LPS and 50 μg/ml ox-LDL for 48 h The blank group was incubated with fresh medium, while the model received 1 μg/ml LPS and 50 μg/ml ox-LDL alone. Subsequently, stained by Oil Red O Staining Kit. After fixated with 4% paraformaldehyde, lipid droplets could be observed under the optical microscope.

2.3.8. Lipid-adjustment experiment

The cell culture medium was collected centrifugated (1,000 g, 20 min) to obtain the supernatant. Washed cells with PBS and isopropyl alcohol was added as extraction solution (1 ml isopropyl alcohol per 5 million cells). Scraped by a cell scraper then transferred the cell suspension to EP tube, and dispersed cells by ice bath ultrasonication (300 W, ultrasound for 2 s, interval for 3 s, total 3 min). The cell lysate was obtained to be measured by centrifugation (10,000 g, 10 min). The content of TC in cell culture medium and cell lysate of each group was determined by the TC Content Assay Kit.

2.3.9. Hemorrhagic risk assessment

For the purpose of evaluation on the hemorrhagic risk of HV-LK loaded HMTL@PM, BALB/c mice were chosen for the tail bleeding experiment. Divided the mice into four groups at random ($n = 3$) and anesthetized, then the mice were intravenously injected through the tail vein (saline, HV, LK and HMTL@PM). Half an hour later, a sharp lancet was used to cut off about 1 cm from the tail end, then promptly immersed in prewarmed saline. The time at which spontaneous bleeding stopped was recorded.

2.4. In vivo studies

2.4.1. Establishment and treatment of atherosclerotic mice

Followed by a three-month high-fat diet, ApoE-/- mice developed into the atherosclerotic mice and assigned to five groups at random ($n = 5$). While the other groups received treatments with HV, LK, HMTL, and HMTL@PM (ATU: 120 U/g), the model group were given saline. All formulations were administered at one-d interval for a treatment cycle of 14 d and the high-fat feed was replaced with a normal feed during treatment.

2.4.2. Thrombus-targeting and biodistribution analysis

Using ICG-labelled HMTL and ICG-labelled HMTL@PM, we examined the thrombus-targeting ability and tissue biodistribution of HMTL@PM in atherosclerotic mice. Atherosclerotic mice were assigned to three groups at random ($n = 3$) and injected with ICG, ICG-labelled HMTL or ICG-labelled HMTL@PM (ICG: 4 mg/kg). At predefined timepoints, the mice were anesthetized by isoflurane inhalation for *in vivo* fluorescence imaging. Furthermore, the main organs and the aortas were removed for fluorescence imaging at the time point of the strongest fluorescence signal. All of the MFI were analyzed by Living Image software. Then the fresh heart and aortic tissues were collected for a frozen longitudinal

section of the aortic valve in order to further investigate the thrombus-targeting ability of HMTL@PM.

2.4.3. *Oil red O staining of aorta*

Euthanized the atherosclerotic mice, the aortas were removed and fixated in 4% paraformaldehyde after excising the residual adipose tissue and connective tissue on the adventitia of vessels. Stained the plaques within the aortas by Modified Oil Red O Staining Kit. After rinsing with PBS, the aortas were soaked in the oil red O working solution and boiled preheated at 100 °C for 1 h, then washed repeatedly with ddH_2O until the solution is pale pink or colorless. At last, carefully dissect the entire aorta longitudinally, laying it flat on a white background to take a photo and the plaque area was quantified using ImageJ software.

2.4.4. *Serum biochemical test*

After the 2-week treatment cycle, blood was collected from the atherosclerotic mice and centrifuged (3,000 g, 10 min). Collected the supernatant and determined the levels of blood lipids including total cholesterol (TC), high-density lipoprotein cholesterol (HDL-c), triglycerides (TG) and low-density lipoprotein cholesterol (LDL-c) were assayed in each sample. Moreover, the levels of IL-10, IL-6, IL-1α, TNF-α, IL-1β, IFN-γ, MCP-1, iNOS, VEGF and α-SMA in the serum were detected using ELISA kit.

2.4.5. *Histology and immunohistochemistry of the aortic roots*

For the histology, aortas of each group were removed and fixated after treatment. Afterwards, H&E and Masson's trichrome were applied to stain the paraffin sections of aortic roots. Sections were treated with antibodies against CD68 and α-SMA in preparation for the immunohistochemical assay. The semiquantitative analysis was calculated by ImageJ software.

2.4.6. *Safety evaluation*

Body weight of atherosclerotic mice was recorded within 14 d Following treatment, collected the whole blood and removed the main organs including heart, lung, kidney, spleen and liver. Blood routine examination and H&E staining were conducted so as to evaluate the biocompatibility *in vivo*.

3. Results and discussion

3.1. *Basic characterization of HMTL@PM*

3.1.1. *Morphological characterization*

As shown in Fig. 2B, HMTL revealed a uniform particle size of roughly 50 to 70 nm, appeared spherical and generally dispersed. Platelet membrane exhibited a particle size around 200 nm and presented a structure of nano-bubble (Fig. 2C). It provided evidence of the effective encapsulation of PM at the outer layer of HMTL (Fig. 2D). The hydrated particle size of HMTL, PM, and HMTL@PM were 133 ± 9.83, 256.83 ± 37.58 and 154.1 ± 11.36 nm, respectively. (Fig. 2E). The particle size increased after PM coating, which further indicated the successful encapsulation. Moreover, it depicted that the high negative electrical characteristics of the platelet membranes contributed to the surface charge of the HMTL@PM (−29.8 ± 0.9 mV), which was much more negative than that of HMTL (−13.83 ± 2.8 mV). Encapsulation may enhance the stability of HMTL@PM, as indicated by the greater absolute value of the *zeta* potential, which was linked to a more stable system. Furthermore, platelet membrane fragments were formed after freeze-thaw circulation and ultrasound, and the membrane fusion was achieved after coating with nanoparticles. Therefore, the hydrated particle size of HMTL@PM was higher than that of HMTL and smaller than that of the PM alone.

3.1.2. *Verification of the platelet membrane coating*

Constructing biomimetic nanoplatforms is essential to studying drug biocompatibility and active targeted delivery. In this work, HMTL was encapsulated using platelet membranes to prepare biomimetic HMTL@PM. As shown in Fig. 2F, there were no protein bands in the HMTL group, and the protein bands of HMTL@PM group matched that of PM group, indicating that HMTL@PM completely retained the membrane protein on platelet membrane. Platelet surface contains a variety of membrane proteins, glycoprotein like GPVI and GPIbIX-V are widely believed to be a necessary factor in the formation of platelet aggregation on collagen surface under the action of blood flow [40]. CD47 can bind to the SIRP-α on the surface of macrophages, and cause tyrosine phosphorylation in the immunoreceptor tyrosine inhibitory motif, then lead to dephosphorylation of downstream pathway proteins, finally inhibit macrophage phagocytosis [41]. In addition, the sample strip of PM and HMTL@PM was compared with Marker strip. The WB results was shown in Fig. S1. It indicated that HMTL@PM still retained the membrane protein on PM even after ultrasonic cavitation, which proved that HMTL@PM probably possessed the possibility of thrombus targeting adhesion and immune escape function in composition.

3.1.3. *Assessment of drug loading capacity and encapsulation efficiency*

The UV spectra of HV, LK, tannic acid and Mn^{2+}-tannic acid complex at 200–600 nm were investigated, and the results were shown in Fig. 2G. The maximum absorption wavelength of tannic acid redshifted from 278 to 350 nm after the formation of complex with Mn^{2+}. The standard curve 1 ($y = 0.0242x+0.0189$, $R^2=0.9997$) of absorbance of Mn^{2+}-tannic acid complex with different gradient concentrations at 350 nm is considered for quantitative analysis (Fig. S2). Similarly, Mn^{2+}-tannic acid complex with different concentration gradients was set up for determination of BCA protein concentration, then the standard curve 2 ($y = 0.007246x-0.01165$, $R^2=0.9989$) was established (Fig. S3). The interference of tannic acid on the determination of total protein was eliminated by combining the two standard curves. The content of LK was detected by Luminescent Kinase Assay Kit, the standard curve 3 of ATP and standard curve 4 of LK was established as shown in Fig. S4 and Fig. S5.To optimize the drug loading conditions of HMTL@PM, the hydrated size and *zeta* potential of HMTL with different polypeptide/polyphenol mass ratios were shown in Fig. S6. As the tannic acid ratio increased, the particle size of HMTL kept growing. When the polypeptide/polyphenol

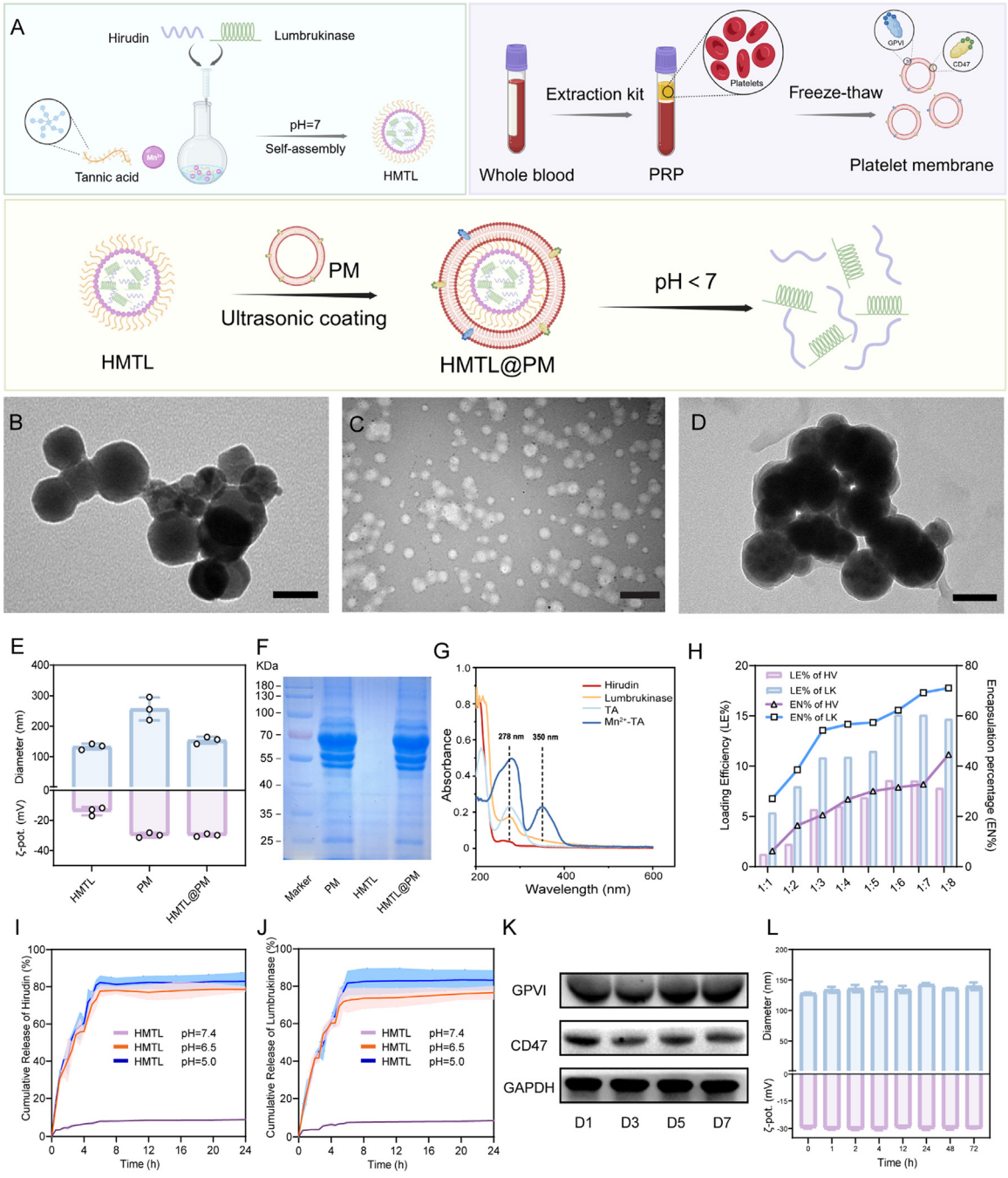

Fig. 2 – Construction and characterization of HMTL@PM: (A) The construction of HMTL@PM; (B) TEM of HMTL, scale bar: 50 nm; (C) TEM of PM, scale bar: 500 nm; (D) TEM of HMTL@PM, scale bar: 100 nm; (E) The particle size and zeta potential of HMTL, PM and HMTL@PM; (F) SDS-PAGE analysis of PM, HMTL and HMTL@PM; (G) UV–Vis-NIR absorption spectrum of HV, LK, tannic acid and Mn^{2+}-TA; (H) The drug loading and encapsulation efficiency of HMTL with various peptide/polyphenol mass ratios; (I, J) Cumulative release of HV or LK from HMTL@PM at various pH (5.0, 6.5, 7.4); (K) Stability of GPVI and CD47 on platelet membrane during 1-wk storage (1 d, 3 d, 5d and 7 d) (n = 3);(L) Stability of HMTL@PM in DMEM with 10% FBS during 72 h storage (n = 3).

mass ratios at 1:1, 1:2, 1:3, 1:4, 1:5 and 1:6, they did not fluctuate much, around 133.03 ± 9.83 nm and −15.47 ± 1.72 mV, respectively. When the polypeptide/polyphenol mass ratio increased to 1:7 and 1:8, the *zeta* potential remained about −15.47 ± 1.72 mV, while the particle size reached about 321.27 ± 23.79nm. Fig. 2H demonstrated that within a certain range, as the amount of tannic acid increased, the drug loading and encapsulation efficiency of HV and LK increased as well. When the polypeptide/polyphenol mass ratio reached 1:6, the drug loading of HV and LK

exhibited the highest, and the encapsulation efficiency was moderate. The drug loading of HV and LK was 8.31% ± 0.44% and 14.95% ± 0.25%, the encapsulation efficiency was 31.45%± 1.35% and 62.29% ± 2.91% repectively. The mixture ratio of polyphenol/peptide was evaluated by combining the drug loading and encapsulation rate of HV and LK, and the optimal ratio 1:6 was obtained through screening. Moreover, the loading efficiency of Mn^{2+} in HMTL@PM was 2.15% ± 0.06%. The standard curve of Mn^{2+} was shown in Fig. S7.

3.1.4. *Release profiles* in vitro *of HV-LK loaded HMTL@PM*

The release profiles of HV and LK were shown in Fig. 2I and 2J. Under normal conditions (pH 7.4), the release of HV and LK from HMTL within 24 h was 8.77% ± 0.38% and 8.43% ± 0.39%, respectively, indicating relative stability of the formulation under normal physiological conditions. In pH 6.5, the release ratio reached 78.64% ± 1.50% and 76.53% ± 6.68% within 24 h, respectively, which significantly increased compared to normal physiological conditions. Within macrophage lysosomes (pH 5.0), due to stronger acidity, more tannic acid-metal complexes dissociated thus resulting in a release of HV and LK at levels of 82.84% ± 5.00% and 83.20% ± 5.35% within 24 h, slightly higher than that at pH 6.5. The results indicated that HMTL possessed excellent pH-responsive capacity and had the potential to release HV and LK in simulated acidic pathological microenvironments at atherosclerotic plaque sites. Phenolic compounds contain a large number of dihydroxyphenyl or trihydroxy phenyl groups, which have high π electron content and aromaticity, providing an effective negative binding site for cation-π interactions to form cations, self-assembly to form MPN, the coordination effect will be weaken under acidic conditions by the regulation of pH [42]. The researchers mixed different metal ions with various natural polyphenols to prepare a large number of different kinds of MPN to achieve the pH-responsive release. Guo has previously reported the pH-dependent behavior of coordination between Fe^{3+} and TA [43]. Yin has developed a tannin-assisted biomineralization strategy to encapsulate the protein drugs by complexing TA and Mn^{2+} to selectively dissociate and release the drug in an acidic tumor environment [44]. Similarly, this study relied on the complexation of TA with Mn^{2+} through coordination bonds, which allowed HMTL to form rapidly and disassemble in response to pH.

3.1.5. *Stability test*

GPVI and CD47 protein were selected for WB experiments, the results were shown in Fig. 2K. We also conducted a semi-quantitative analysis of WB results in Fig. S8. The results showed that there was no significant difference in platelet membrane protein content during the 1-wk storage. The particle size and *zeta* potential did not significantly alter over one month, implying that the HMTL@PM was stable during storage (Fig. S9). Furthermore, HMTL@PM was also be stable in the serum-containing medium within 72 h, suggesting that it might show favorable stability in the blood (Fig. 2L). The drug content in HMTL@PM solution to determine whether the HV or LK was leaking. The results were shown in Fig. S10. The results showed that a small amount of HV and lumbrokinase were detectable in the HMTL@PM solution within 1 wk, and the levels increased slightly with prolonged storage. >90% of the drugs were encapsulated in the nanoparticles and remained stable. The results above showed that HMTL@PM possess good stability.

3.2. *Specific thrombus-targeting and selective inflammatory cells uptake*

3.2.1. *Thrombus-targeting and biodistribution analysis*

Following administration at a certain time point, atherosclerotic mice received *in vivo* fluorescence imaging. (Fig. 3A). The results were shown in Fig. 3B and 3F. *Ex vivo* fluorescence distribution of liver, spleen, lung, kidney, aorta and heart after treatment with ICG, ICG-labelled HMTL or ICG-labelled HMTL@PM for 6 h were shown in Fig. 3C and 3G The mice treated with ICG and ICG-labelled HMTL showed systemic distribution, most of the fluorescence signals were concentrated in liver, less in spleen, lung and kidney. ICG-labelled HMTL@PM presented a time-dependent targeting distribution, and the aorta near the heart exhibited the obvious fluorescence signals within the first 6 h, suggesting that the accumulation of biomimetic nanoparticles at the plaque site gradually increases with time and reaches a peak value at 6th h, while the fluorescence at the plaque site decreases at the 8th h due to metabolic excretion. The frozen longitudinal sections were shown in Fig. 3D, and the quantitative average fluorescence intensity was shown in Fig. 3H. The results showed that compared with the HMTL group, HMTL@PM could effectively reach the site of aortic valve, that is, the site of atherosclerotic lesions. On the basis of *in vivo* and *in vitro* fluorescence imaging results, this study further fully demonstrated the thrombus-targeting ability of HMTL@PM, and provided support for the release of encapsulated drugs in its anti-atherosclerotic therapy. The above results indicated that the platelet membrane-coated HMTL@PM possessed a good ability to actively target thrombus and accumulate in plaques.

3.2.2. *Selective uptake of HMTL@PM by activated platelets and inflammatory cells*

The binding affinity of HMTL@PM to activated platelets was assessed. The results showed that after HMTL@PM treatment, the green fluorescence in platelets was stronger than that in HMTL treatment group, indicating the potential of HMTL@PM targeting activated platelets (Fig. S11). For utilization in AS therapy, the ability of HMTL@PM to be uptake and function efficiently inside is significant [45]. Additionally, we also explored the uptake of HMTL@PM by normal and LPS-stimulated cells due to the inflammatory microenvironment of atherosclerosis. The comparative analysis of the uptake of ICG-labelled HMTL and ICG-labelled HMTL@PM by RAW264.7, HUVEC, LPS-stimulated RAW264.7 and LPS-stimulated HUVEC was shown in Fig. 3E, the mean fluorescence intensity was calculated (Fig. 3I and 3J). For normal cells, ICG-labelled HMTL@PM showed a steady rise in the average fluorescence intensity in HUVEC comparing to ICG-labelled HMTL, while there is no significance in RAW264.7. For LPS-stimulated, the uptake of ICG-labelled HMTL@PM was significantly greater

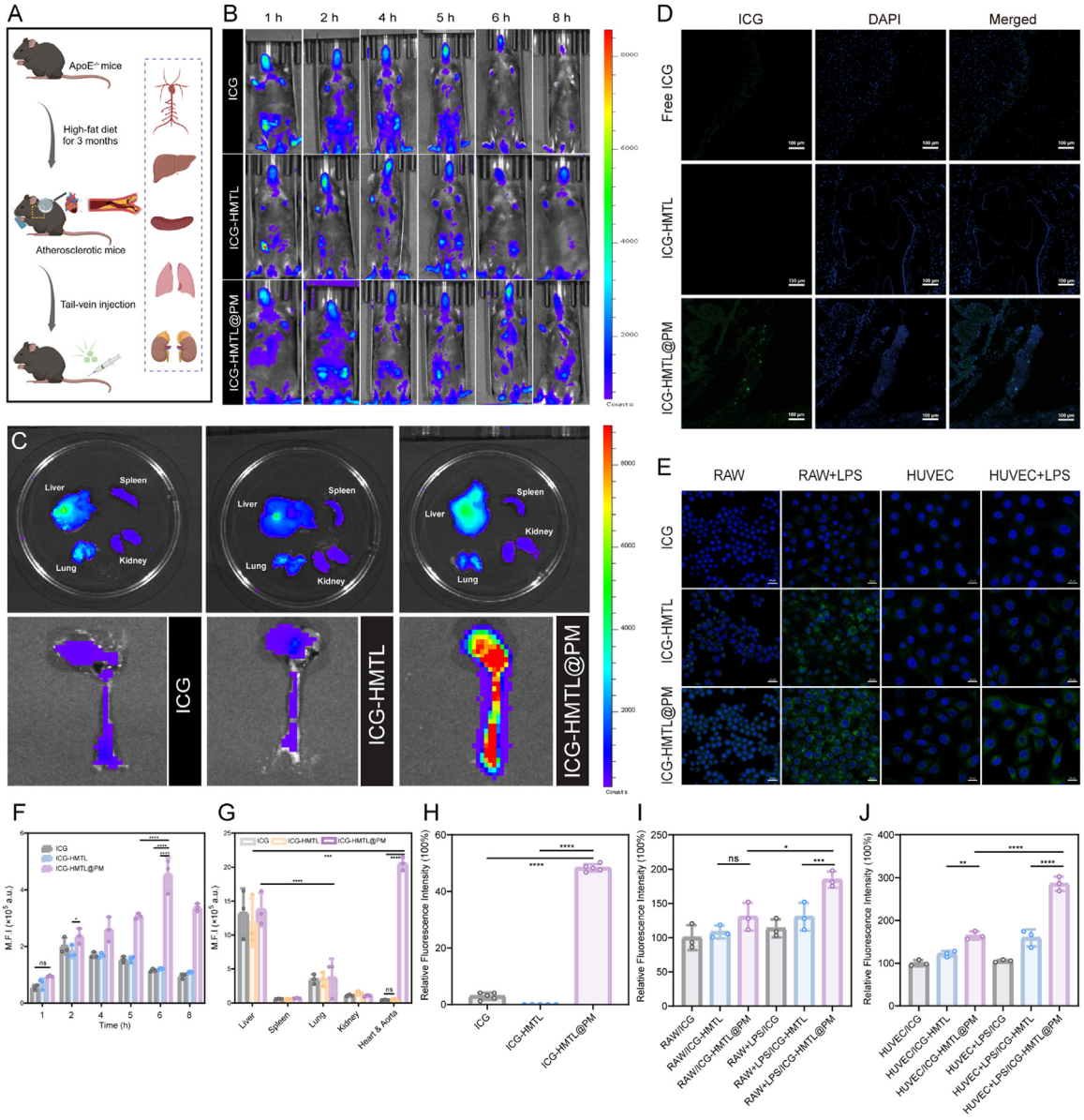

Fig. 3 – Specific thrombus-targeting and selective inflammatory cells uptake. (A) Establishment atherosclerotic mice and *in vivo* fluorescence imaging; (B) Targeted thrombus fluorescence imaging experiments of ICG, ICG-labelled HMTL or ICG-labelled HMTL@PM at consecutive time points; (C) Fluorescence distribution images of liver, spleen, lung, kidney, aorta and heart after treatment with ICG, ICG-labelled HMTL or ICG-labelled HMTL@PM for 6 h; (D) Frozen longitudinal section of the tricuspid valve, scale bar: 100 μm;(E) Cellar uptake of ICG, ICG-labelled HMTL or ICG-labelled HMTL@PM in RAW264.7, activated RAW264.7, HUVEC and activated HUVEC. Scale bar: 20 μm; (F) Quantitative average fluorescence intensity of mice *in vivo*; (G) Quantitative average fluorescence intensity of main organs and aortas *ex vivo*; (H) Quantitative average fluorescence intensity of frozen longitudinal section ($n = 5$); (I, J) Quantitative average fluorescence intensity in RAW264.7 and HUVEC.

than that of ICG-labelled HMTL, contributing to the platelet membrane's strong affinity for inflammatory cells. In general, inflammatory cells more selectively ingested and efficiently absorbed HMTL@PM. Platelets exhibit a high affinity for inflammatory macrophages, with specific receptor-ligand interactions facilitating improved uptake. Platelets possess numerous receptors, including P-selectin, E-selectin, and GPIIb/IIIa, which can interact with ligands on the surface of macrophages, such as P-selectin glycoprotein ligand-1 (PSGL-1) and integrin. This interaction enables platelets to adhere to inflammatory macrophages [46–48].

3.3. *Anti-inflammatory capacity*

Inflammation-alleviation is essential to AS management since it is a typical chronic inflammatory disease [49–51].

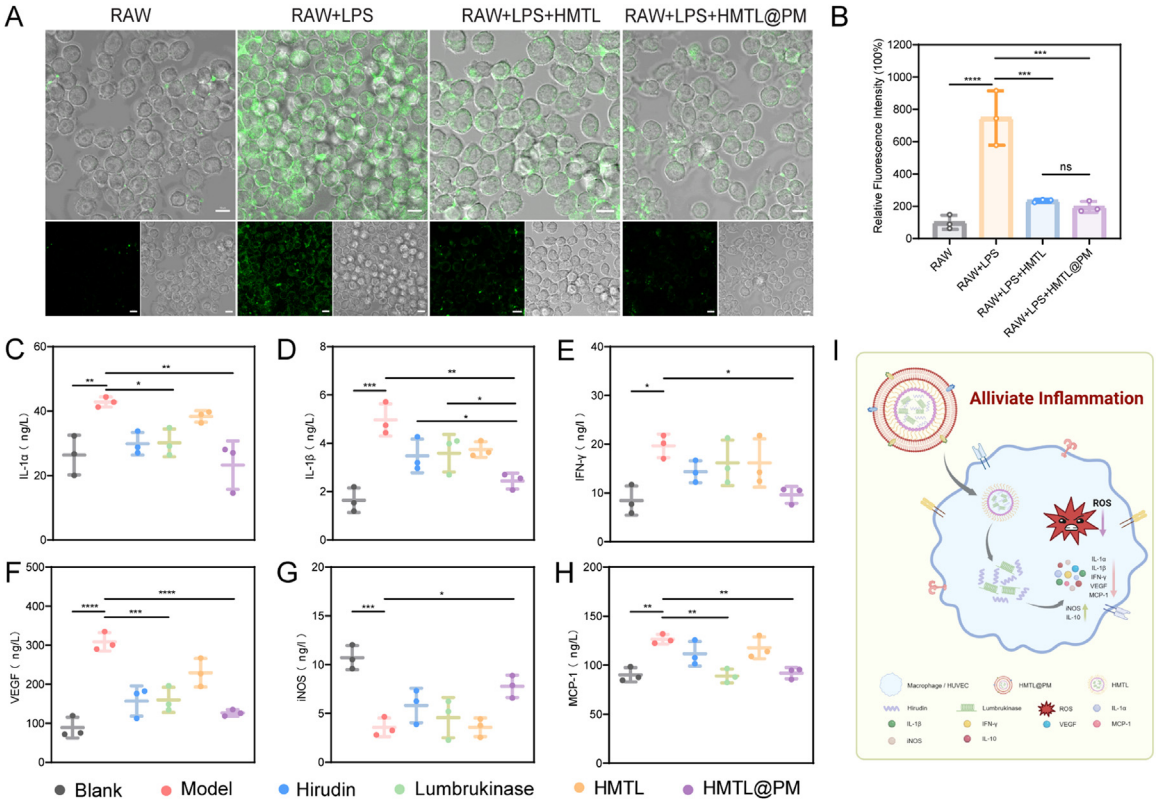

Fig. 4 – ROS-scavenging and anti-inflammatory capacity of HMTL@PM. (A) Intracellular ROS level in RAW264.7 or activated RAW264.7 after treatment with PBS, HMTL or HMTL@PM. Scale bar: 10 μm; (B) Quantitative average fluorescence intensity; (C–H) Levels of cytokines detected by ELISA after different treatment, including IFN-γ, IL-1α, IL-1β, VEGF, MCP-1 and iNOS. (I) Anti-inflammatory process of HMTL@PM.

Overproduction of ROS will bring out oxidative stress, which subsequently damages cells and ultimately causes inflammation. Therefore, the ROS-scavenging effect of HMTL@PM was investigated (Fig. 4A and 4B). ROS was rarely produced in normal macrophages and the levels of ROS were greater in LPS-stimulated cells. Whereas the green fluorescence of macrophages was significantly weakened after co-incubation with HMTL or HMTL@PM, indicating that the preparation had good ROS clearance ability. However, there was no significant difference in HMTL and HMTL@PM. Based on the analysis of cell uptake, it may be that macrophages own a good ability to uptake nanoparticles, thus decreased intracellular ROS levels had no significant effect on whether or not the platelet membranes were coated. Furthermore, Levels of cytokines detected by ELISA after different treatment, including TNF-α, IL-1α, IFN-γ, IL-1β, IL-10, iNOS, MCP-1, α-SMA and VEGF, were shown in Fig. 4C–4H and Fig. S12. HMTL@PM significantly lowered the levels of IL-1α, IL-1β and IFN-γ, which are pro-inflammatory cytokines, thus alleviating inflammation. Studies have suggested that IL-1β is the latter being a major pro-inflammatory mediator of AS [52]. As the results shown in Fig. 4D, compared with HV and lumbrokinase monotherapy, HMTL@PM group could significantly reduce the levels of anti-inflammation factor IL-1β, which indicated HMTL@PM possessed great anti-inflammatory capacity. Decreased MCP-1 content thus decreased the tendency of monocytes to the site of inflammation; VEGF levels were decreased to inhibit angiogenesis. To a certain extent, iNOS levels were increased to promote NO production and platelet aggregation was prevented. TNF-α, IL-10 and α-SMA were not significantly affected. Overall, the anti-inflammatory process of HMTL@PM was shown in Fig. 4I.

3.4. *Evaluation of thrombolysis ability*

3.4.1. In vitro *clot lysis test*

As shown in Fig. 5A, following incubation, the solution containing HMTL (pH=5) appeared a noticeable turbidity in the supernatant, and the volume of blood clot was considerably decreased. The mass of the clot was weighed both before and after the therapy to determine the thrombolytic efficiency. In contrast to PBS, HV, LK, HMTL (pH 7.4), HMTL@PM, the dissolution efficiency of HMTL (pH 5) group exhibited the highest, about 62.12% ± 4.11%. Both HV and LK were thrombolytic to a certain extent, and the thrombolytic rate of HMTL is significantly higher than that of monotherapy (Fig. 5B). A similar trend could be observed in the amount of hemoglobin and fibrin in the supernatant following clot lysis. (Fig. 5C).

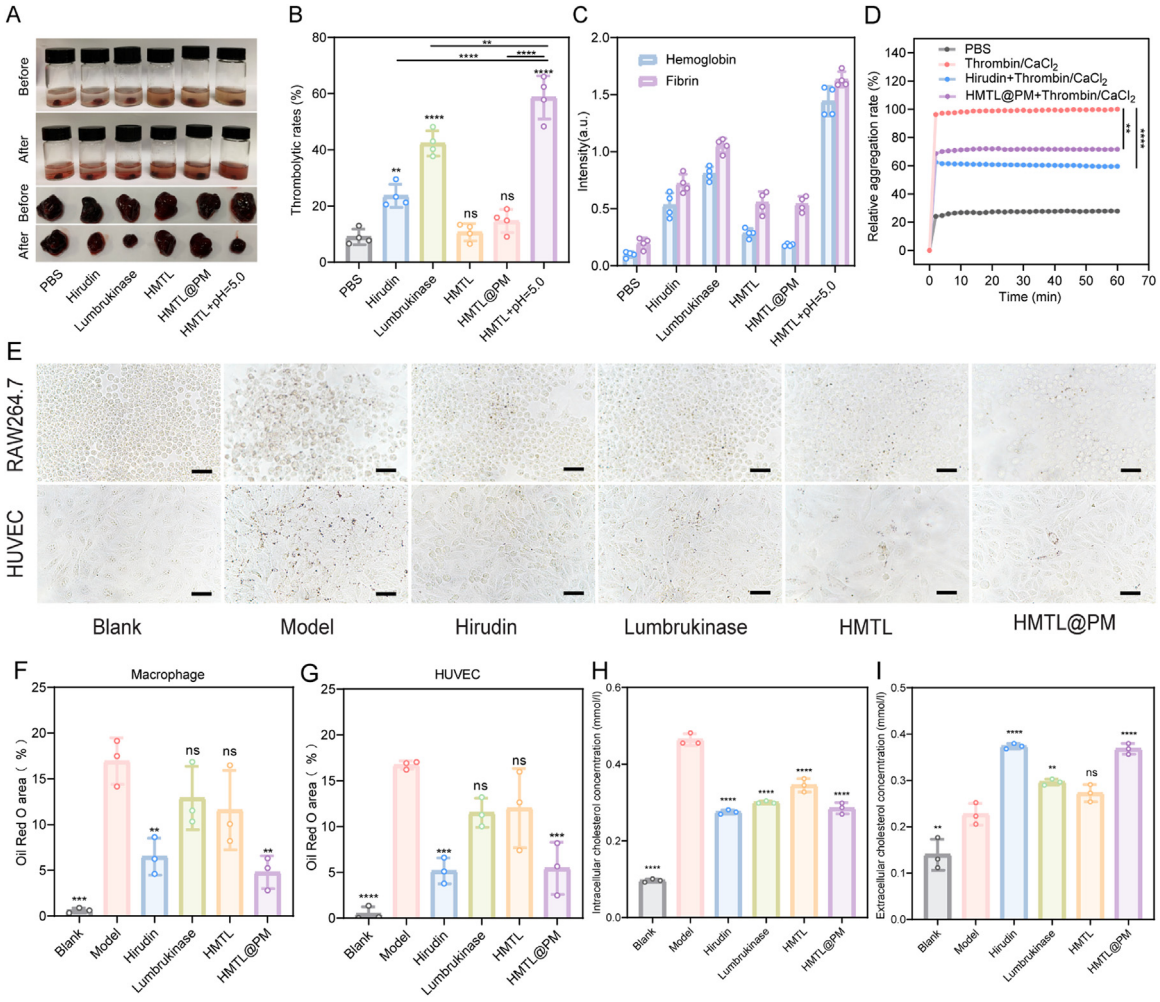

Fig. 5 – Evaluation of thrombolysis ability. (A) Images of changes in blood clot and supernatant after treatment with PBS, HV, LK, HMTL, HMTL@PM or HMTL+pH=5; (B) Thrombolytic rates after different treatments; (C) Hemoglobin and fibrin absorbance following treatments; (D) Platelets aggregation rate after treatment with various groups, including PBS, thrombin/$CaCl_2$, HV or HMTL@PM; (E) Oil red staining was performed after different preparation interacted with foam cell. Scale bar:100 μm; (F) Analysis of oil red staining in RAW264.7 quantitatively; (G) Analysis of oil red staining in HUVEC quantitatively; (H) Intracellular cholesterol content after different treatment interacted with foam cells; (I) Extracellular cholesterol content after different treatment interacted with foam cells.

3.4.2. *Anticoagulant effect assay*

As shown in the Fig. 5D, when incubated with Thrombin/$CaCl_2$, platelets appeared rapid aggregation. During the incubation with HV, the platelet aggregation rate of HMTL@PM was lower, indicating that HV successfully prevented platelet activation, thus ameliorated blood clot formation.

3.4.3. *Effects of HMTL@PM on foam cell formation*

One of the primary characteristics of atherosclerotic lesions is the formation of foam cells [53–56]. Consequently, we stained the intracellular lipid droplets then investigated whether HMTL@PM therapy could decrease the formation of foam cell (Fig. 5E). RAW 264.7 and HUVEC subjected to LPS and ox-LDL treatment displayed a considerable increase of intracellular lipid droplets in cells. Additionally, foam cells performed attenuation following varying treatment. In addition, *via* treatment with HV and HMTL@PM, the development of foam cell formation could be dramatically inhibited (Fig. 5F and 5G).

3.4.4. *Lipid-adjustment experiment*

The formation and accumulation of lipid foam cells promote the occurrence and development of atherosclerosis [57]. Therefore, the cholesterol contents inside and outside the foam cells were detected respectively, and the results were shown in Fig. 5H and 5I. The intracellular cholesterol content of the model group was higher, indicating that the foam cells engulfed a large amount of ox-LDL. Compared with model group, HV group, LK group, HMTL group and HMTL@PM group all promoted cholesterol efflux to different extent. The intracellular cholesterol content of HMTL@PM

groups showed a significant decrease trend, while the extracellular cholesterol content was significantly increased, which indicated that HMTL@PM could promote cholesterol efflux in foam cells to regulate lipid metabolism, and its regulatory effect was better than that of HV or LK alone.

3.5. *Evaluation of anti-atherosclerosis effects* in vivo

3.5.1. *Oil red O staining of aorta*

The atherosclerotic mice were successfully established with high-fat diet and treated with HMTL@PM for 14 d as shown in Fig. 6A. Using oil red O to stain the gross diseased area of the aorta, so as to evaluate the anti-atherosclerosis therapeutic effect of HMTL@PM *in vivo*. The quantitative analysis of the staining results and staining area was shown in Fig. 6B. The model group showed more stained areas in general, while the stained areas of HV group, LK group, HMTL group and HMTL@PM were reduced to varying degrees, indicating that each group had an inhibitory effect on the formation and development of atherosclerotic plaques. Further quantization of the staining area of oil red O indicated that the biomimetic nanoparticles HMTL@PM could significantly reduce the lesion area of atherosclerotic plaque thus ameliorate thrombus (Fig. 6C).

3.5.2. *Serum biochemical test*

The contents of TC, HDL-c, TG, and LDL-c in serum of atherosclerotic mice after treatment were respectively detected, and the results were shown in Fig. 6D-6G. Compared with HV, LK or HMTL group, HMTL@PM could significantly reduce the contents of TC, HDL-c, TG, and LDL-c in blood, especially the content of TG, but has little effect on the content of HDL-c. Therefore, HMTL@PM could significantly reduce blood lipid, which was conducive to reducing the uptake of ox-LDL by inflammatory cells, thereby reducing the foam cells formation to inhibit the development of AS. Serum cytokine levels in each group were detected by ELISA, and the detection results were displayed in Fig. 6H and S13. HMTL@PM could significantly reduce the contents of pro-inflammatory factors IL-1α, IL-6, IL-1β, IFN-γ, MCP-1 and VEGF, and to a certain extent increase the levels of anti-inflammatory factors IL-10 and iNOS. The pro-inflammatory factors TNF-α and α-SMA were not significantly affected. The levels of serum inflammatory factors were decreased in LK group and HV alone group, but the efficacy was less than that in HMTL@PM group.

3.5.3. *Histology and immunohistochemistry of the aortic roots*

For the purpose to examine the composition of atherosclerotic plaques, histochemical analysis of aortic root sections was performed (Fig. 6I–6L). H&E stain revealed the vascular plaque's location, and compared to the saline group, the HMTL@PM group's plaque area was significantly smaller. Moreover, in the HMTL@PM group, there was more collagen surrounding the plaques, as shown by Masson's trichrome staining. In addition, anti-CD68 staining demonstrated that treat with HMTL@PM could successfully decreased macrophage infiltration. α-SMA antibody staining revealed a significant accumulation of smooth muscle cells in the HMTL@PM group's aortic roots, which was thought to be advantageous for atherogenesis. To sum up, HMTL@PM therapy may increase smooth muscle cell recruitment, decrease macrophage infiltration, inhibit inflammatory factor expression and plaque development, thus ameliorate the progression of AS.

3.6. *Safety evaluation*

3.6.1. *Biocompatibility assay*

Fig. 7A showed that in comparison to the positive group, the hemolysis rate of HMTL@PM was below 5%, demonstrating outstanding hemocompatibility. Additionally, compared to thrombin/$CaCl_2$, HMTL@PM will not induce platelet aggregation leading to thrombus over time (Fig. 7B).

3.6.2. *Hemorrhagic risk assessment*

The hemorrhagic risk of HMTL@PM was further assessed through the measurement of tail-vein bleeding time. As shown in Fig. 7C, because of the blood system's inherent hemostatic properties, mice treated with PBS could be observed complete blood coagulation approximately 3 min after bleeding. Administration of free HV or lumbrokinase, the tail bleeding time was significantly prolonged, suggesting that its fibrinolytic activity was strong and accompanied with non-specific bleeding side effects. The tail bleeding time was significantly different in HMTL@PM-treated atherosclerotic mice from those in HV and LK-treated atherosclerotic mice, which means the HMTL@PM could reduce the side effects of HV and LK thus minimize the hemorrhagic risks.

3.6.3. *Evaluation of cell toxicity*

Macrophages and endothelial cells are related to the progression of atherosclerosis, the safety of HMTL and HMTL@PM was assessed. As shown in Fig. 7D and S14, the assay showed that the viability was all better than 90% after incubation with various concentration of HMTL or HMTL@PM. On the one hand, the encapsulation of polypeptides mediated by tannic acid, a natural polyphenolic compound, can stay away from the toxic side effects caused by the use of chemical crosslinking agents; on the other hand, platelet membrane confers high biocompatibility, thereby reducing any toxicity. Hence, HMTL@PM were not significantly cytotoxic, and the platelet membranes coating further enhanced cell safety.

3.6.4. *Safety assay* in vivo

Changes in weight of mice during the treatment showed that the body weight did not fluctuate significantly in each group and showed a trend of continuous increase (Fig. S15). Furthermore, all index from the clinical biochemical analysis and complete blood count were within the normal range. The leukocyte index of HMTL@PM group was significantly lower in contrast to the saline group, indicating that the treatment relieved inflammation of atherosclerotic mice (Fig. 7E-7L). In the H&E sections of all treatment groups, it showed no obvious damage, with the exception of the saline group, whose liver sections showed fatty vacuoles as a result of constant high-fat diet feeding. (Fig. 7M). In conclusion, it suggested that HMTL@PM administration was safe at the study-tested dosage.

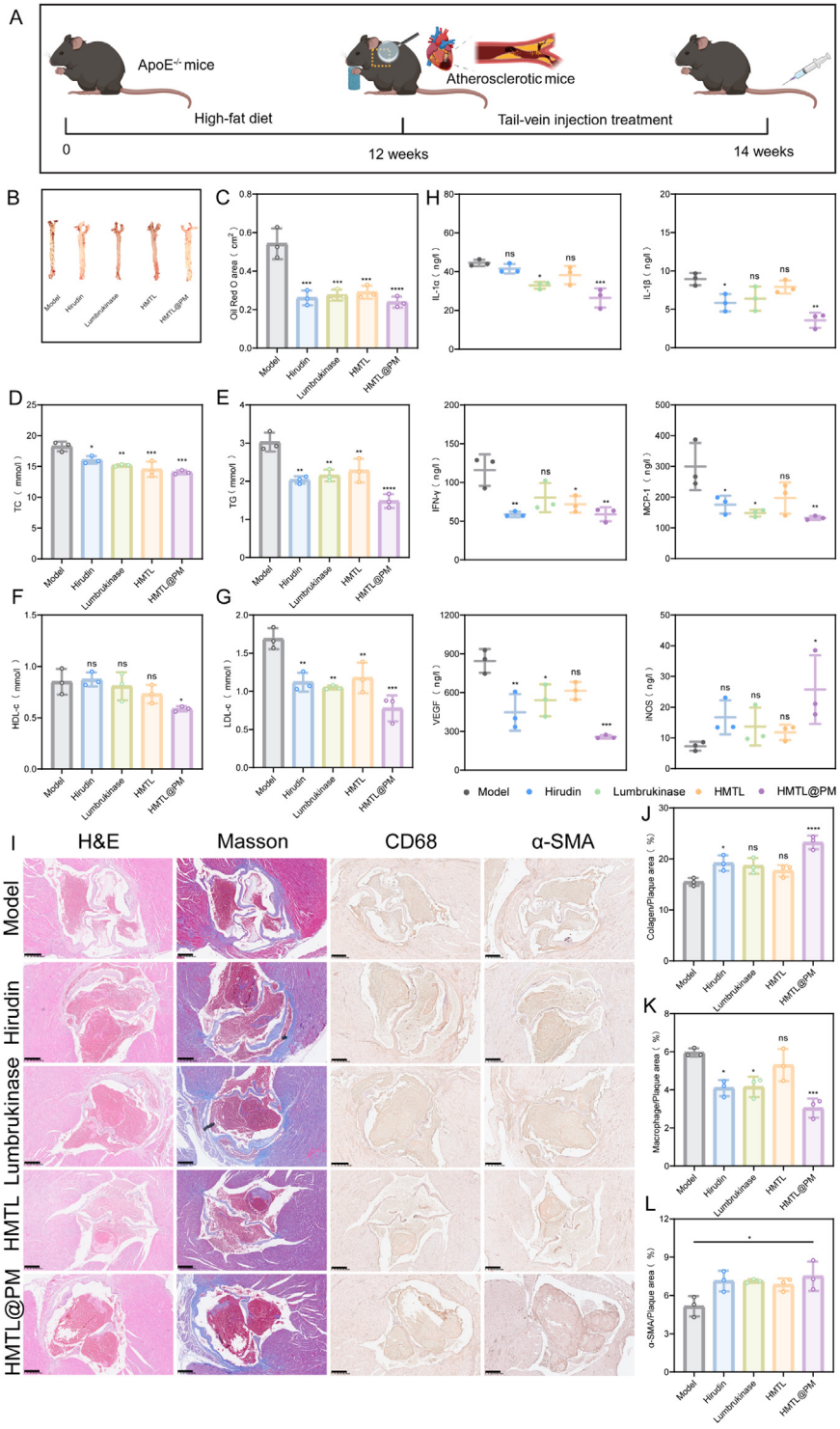

Fig. 6 – Evaluation of anti-atherosclerosis ability *in vivo*. (A) Establishment and treatment of atherosclerotic mice; (B) Oil red O staining of aorta after different treatments; (C) Analysis of oil red O staining quantitatively; (D-G) Levels of blood fat, including TC, HDL-c, TG, and LDL-c; (H) Cytokine levels of atherosclerotic mice after treatment with different treatment, including IL-1α, IL-6, IL-1β, IFN-γ, VEGF, MCP-1, and iNOS; (I) H&E, Masson, anti-CD68 and α-SMA staining of aortic root after different treatments. Scale bar:250 μm; (J) Analysis of Collagen/Plaque area quantitatively; (K) Analysis of Macrophage/Plaque area quantitatively; (L) Analysis of α-SMA/Plaque area quantitatively.

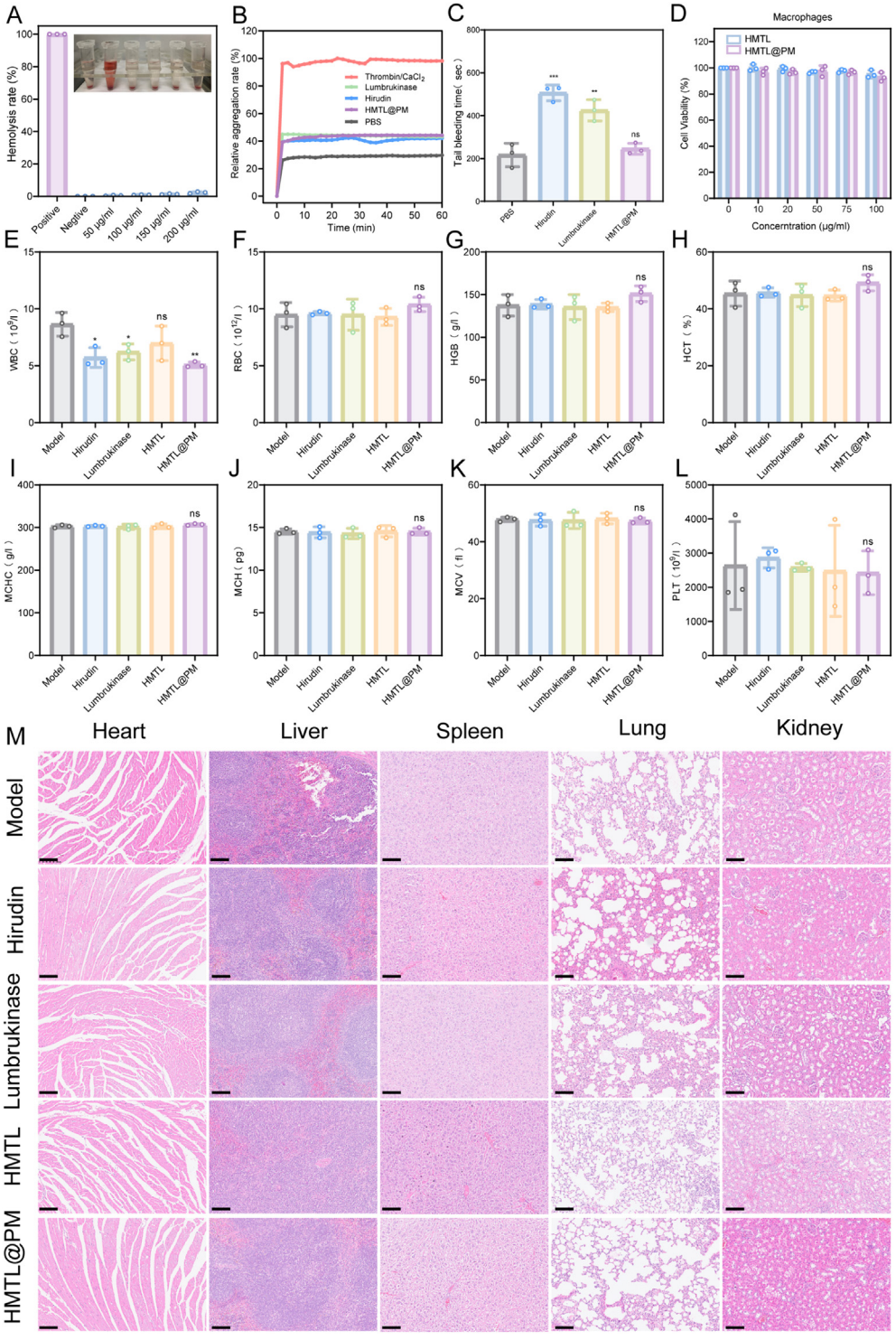

Fig. 7 – Safety evaluation. (A) Hemolysis rate of RBCs after incubation with different concentrations of HMTL@PM (n = 3); (B) Platelet aggregation assay of different groups, including thrombin/$CaCl_2$, LK, HV, HMTL@PM and PBS; (C) Tail-vein bleeding time experiment with different treatments (n = 3); (D) Cell viability of RAW264.7 after treatment with HMTL or HMTL@PM at various concentrations (n = 3); (E-L) The routine blood test of atherosclerotic mice after treatments (n = 3); (M) H&E staining of atherosclerotic mice after treatments. Scale bar: 100 μm.

4. Conclusion

In summary, a novel biomimetic thrombus-targeted nanoparticle HMTL@PM had been successfully developed for co-deliver HV and lumbrokinase, aiming to ameliorate thrombus and inflammation for atherosclerosis therapy. HMTL@PM exhibited controllable drug release in acidic environment with favorable hydrodynamic size. Meanwhile, HMTL@PM could preferentially accumulate at the thrombus site and selectively uptake by inflammatory cells related to the homing effect of platelet membrane. This targeted accumulation effectively curbed the progression of inflammation, which achieved through ROS-scavenging properties and cytokines-regulation. Moreover, leveraging the thrombolysis ability of HV and LK, it manifested efficacious thrombus elimination. Treatment *in vivo* demonstrated HMTL@PM could effectively suppress the development of AS, characterized by tremendous biocompatibility. Overall, the biomimetic thrombus-targeted nanoparticle presented a favorable therapeutic efficacy and hold significant potential for the atherosclerosis therapy.

Conflicts of interest

The authors report no conflicts of interest. The authors alone are responsible for the content and writing of this article.

Acknowledgements

This research was funded by the National Natural Science Foundation of China, grant numbers 82374048 and 82174096, Natural Science Foundation of Zhejiang Province, grant number LZ21H280001.

Supplementary materials

Supplementary material associated with this article can be found, in the online version, at doi:10.1016/j.ajps.2024.100990. The figures and tables with "S" before the serial number are included in the Supplementary material.

References

[1] Bjoerkegren JLM, Lusis AJ. Atherosclerosis: recent developments. Cell 2022;185(10):1630–45.
[2] Libby P. The changing landscape of atherosclerosis. Nature 2021;592(7855):524–33.
[3] Xu S, Ilyas I, Little PJ, Li H, Kamato D, Zheng X, et al. Endothelial dysfunction in atherosclerotic cardiovascular diseases and beyond: from mechanism to pharmacotherapies. Pharmacol Rev 2021;73(3):924–67.
[4] Tamargo IA, Baek KI, Kim Y, Park C, Jo H. Flow-induced reprogramming of endothelial cells in atherosclerosis. Nat Rev Cardiol 2023;20(11):738–53.
[5] Libby P, Buring JE, Badimon L, Hansson CK, Deanfield J, Bittencourt MS, et al. Atherosclerosis. Nat Rev Dis Prim 2019;5(1):56.
[6] Alkarithi G, Duval C, Shi Y, Macrae FL, Ariens RAS. Thrombus structural composition in cardiovascular disease. Arterioscler Thrombos Vasc Biol 2021;41(9):2370–83.
[7] Capodanno D, Alberts M, Angiolillo DJ. Antithrombotic therapy for secondary prevention of atherothrombotic events in cerebrovascular disease. Nat Rev Cardiol 2016;13(10):609–22.
[8] Stark K, Massberg S. Interplay between inflammation and thrombosis in cardiovascular pathology. Nat Rev Cardiol 2021;18(9):666–82.
[9] Vu TK, Hung DT, Wheaton VI, Coughlin SR. Molecular cloning of a functional thrombin receptor reveals a novel proteolytic mechanism of receptor activation. Cell 1991;64(6):1057–68.
[10] Hara T, Fukuda D, Tanaka K, Higashikuni Y, Hirata Y, Nishimoto S, et al. Rivaroxaban, a novel oral anticoagulant, attenuates atherosclerotic plaque progression and destabilization in ApoE-deficient mice. Atherosclerosis 2015;242(2):639–46.
[11] Gadi I, Fatima S, Elwakiel A, Nazir S, Al-Dabet MDM, Rana R, et al. Different DOACs control inflammation in cardiac ischemia-reperfusion differently. Circ Res 2021;128(4):513–529.
[12] Tardif JC, Kouz S, Waters DD, Bertrand OF, Diaz R, Maggioni AP, et al. Efficacy and safety of low-dose colchicine after myocardial infarction. New Eng J Med 2019;381(26):2497–505.
[13] Ridker PM, Everett BM, Thuren T, Macfadyen JG, Chang WH, Ballantyne C, et al. Antiinflammatory therapy with canakinumab for atherosclerotic disease. New Eng J Med 2017;377(12):1119–31.
[14] Gebhard C, Regitz-Zagrosek V. Colchicine in patients with chronic coronary disease. New Eng J Med 2021;384(8):776–7.
[15] Zhu Y, Han HH, Zhai L, Yan Y, Liu X, Wang Y, et al. Engineering a "three-in-one" hirudin prodrug to reduce bleeding risk: a proof-of-concept study. J Control Releas 2021;338:462–71.
[16] Zhang K, Ma Z, Li S, Zhang W, Foda MF, Zhao Y, et al. Platelet-covered nanocarriers for targeted delivery of hirudin to eliminate thrombotic complication in tumor therapy. Acs Nano 2022;16(11):18483–96.
[17] Men Z, Lu X, He T, Wu M, Su T, Shen T. Microneedle patch-assisted transdermal administration of recombinant hirudin for the treatment of thrombotic diseases. Int J Pharm 2022;612:121332.
[18] Li S, Zhang K, Ma Z, Zhang W, Song Z, Wang W, et al. Biomimetic nanoplatelets to target delivery hirudin for site-specific photothermal/photodynamic thrombolysis and preventing venous thrombus formation. Small 2022;18(51):e2203184.
[19] Pan Y, Wang X, Yin Z. Synthesis and evaluation of cationic polymeric micelles as carriers of lumbrokinase for targeted thrombolysis. Asian J Pharmaceut Sci 2019;14(2):144–53.
[20] Liao J, Ren X, Yang B, Li H, Zhang Y, Yin Z. Targeted thrombolysis by using c-RGD-modified N,N,N-trimethyl chitosan nanoparticles loaded with lumbrokinase. Drug Dev Ind Pharm 2019;45(1):88–95.
[21] Huang CQ, Li W, Wu B, Chen WM, Chen LH, Mo GW, et al. Pheretima aspergillum decoction suppresses inflammation and relieves asthma in a mouse model of bronchial asthma by NF-κB inhibition. J Ethnopharmacol 2016;189:22–30.
[22] Cheng MB, Wang JC, Li YH, Liu XY, Zhang X, Chen DW, et al. Characterization of water-in-oil microemulsion for oral delivery of earthworm fibrinolytic enzyme. J Control Releas 2008;129(1):41–8.
[23] Yao Y, Chen H, Barkat A, Liao F, Xiao Y, Zhao Z, et al. A zombie macrophage-based "trojan horse" enhances the effect of efferocytosis through immune regulation for atherosclerosis treatment. Adv Funct Mater 2024:e2315034.
[24] Gao C, Huang Q, Liu C, Kwong CHT, Yue L, Wan JB, et al. Treatment of atherosclerosis by macrophage-biomimetic nanoparticles via targeted pharmacotherapy and

sequestration of proinflammatory cytokines. Nat Commun 2020;11(1):2622.
[25] Zhu YX, Jia HR, Jiang YW, Guo Y, Duan QY, Xu KF, et al. A red blood cell-derived bionic microrobot capable of hierarchically adapting to five critical stages in systemic drug delivery. Exploration (Beijing) 2023;4(2):20230105.
[26] Tao Y, Lan X, Zhang Y, Fu C, Liu L, Cao F, et al. Biomimetic nanomedicines for precise atherosclerosis theranostics. Acta Pharmaceutica Sinica B 2023;13(11):4442–60.
[27] Zhu Y, Xu L, Kang Y, Cheng Q, He Y, Ji X. Platelet-derived drug delivery systems: pioneering treatment for cancer, cardiovascular diseases, infectious diseases, and beyond. Biomaterials 2024;306:122478.
[28] Li X, Zhang Y, Ren X, Wang Y, Chen D, Li Q, et al. Ischemic microenvironment-responsive therapeutics for cardiovascular diseases. Adv Mat 2021;33(52):e2105348.
[29] Li QY, Huang ZY, Pang ZQ, Wang QZ, Gao JF, Chen J, et al. Targeted delivery of platelet membrane modified extracellular vesicles into atherosclerotic plaque to regress atherosclerosis. Chem Engineer J 2023;452(0):138992.
[30] Jiang Y, Wei ZY, Song ZF, Qian HY. Platelet-inspired targeting delivery for coronary heart disease. Heliyon 2024;10(5):e27166.
[31] Guo J, Cui B, Zheng J, Yu C, Zheng X, Yi L, et al. Platelet-derived microparticles and their cargos: the past, present and future. Asian J Pharmaceut Sci 2024;19(2):100907.
[32] Davi G, Patrono C. Platelet activation and atherothrombosis. N Engl J Med 2007;357(24):2482–94.
[33] Zhang LF. Nanoparticles mimicking platelets and platelet cloaking. Blood 2019;134:38.
[34] Wei X, Ying M, Dehaini D, Su Y, Kroll AV, Zhou J, et al. Nanoparticle functionalization with platelet membrane enables multifactored biological targeting and detection of atherosclerosis. ACS Nano 2018;12(1):109–16.
[35] Fontana F, Molinaro G, Moroni S, Pallozzi G, Ferreira MPA, Tello RP, et al. Biomimetic platelet-cloaked nanoparticles for the delivery of anti-inflammatory curcumin in the treatment of atherosclerosis. Adv Healthc Mater 2024;13(15):e2302074.
[36] Yu HT, Palazzolo JS, Zhou JJ, Hu YJ, Niego B, Pan SJ, et al. Bioresponsive polyphenol-based nanoparticles as thrombolytic drug carriers. ACS Appl Mater Interface 2022;14(3):3740–51.
[37] Han YY, Lin ZX, Zhou JJ, Yun G, Guo R, Richardson JJ, Caruso F, et al. Polyphenol-mediated assembly of proteins for engineering functional materials. Angew Chem Int Ed Engl 2020;59(36):15618–25.
[38] Xu WJ, Lin ZX, Pan SJ, Chen JQ, Wang TZ, Cortez-Jugo C, Caruso F. Direct assembly of metal-phenolic network nanoparticles for biomedical applications. Angew Chem Int Ed Engl 2023;62(45):e202312925.
[39] Hu CMJ, Fang RH, Wang KC, Luk BT, Thamphiwatana S, Dehaini D, et al. Nanoparticle biointerfacing by platelet membrane cloaking. Nature 2015;526(7571):118–21.
[40] Moroi M, Jung SM. Platelet glycoprotein VI: its structure and function. Thromb Res 2004;114(4):221–33.
[41] Olsson M, Bruhns P, Frazier WA, Ravetch JV, Oldenborg PA. Platelet homeostasis is regulated by platelet expression of CD47 under normal conditions and in passive immune thrombocytopenia. Blood 2005;105(9):3577–82.
[42] Geng HM, Zhong QZ, Li JH, Lin ZX, Cui JW, Caruso F, et al. Metal ion-directed functional metal-phenolic materials. Chem Rev 2022;122(13):11432–73.
[43] Guo JL, Ping Y, Ejima H, Alt K, Meissner M, Richardson JJ, et al. Engineering multifunctional capsules through the assembly of metal-phenolic networks. Angew Chem Int Ed Engl 2014;53(22):5546–51.
[44] Yin SY, Hu YC, Zheng J, Li JS, Yang RH. Tannic acid-assisted biomineralization strategy for encapsulation and intracellular delivery of protein drugs. ACS Appl Mater Interfaces 2022;14(45):50583–91.
[45] He H, Han Q, Wang S, Long M, Zhang M, Li Y, et al. Design of a multifunctional nanozyme for resolving the proinflammatory plaque microenvironment and attenuating atherosclerosis. ACS Nano 2023;17(15):14555–71.
[46] Zarbock A, Singbartl K, Ley K. Complete reversal of acid-induced acute lung injury by blocking of platelet-neutrophil aggregation. J Clin Invest 2006;116(12):3211–19.
[47] Cauwenberghs N, Vanhoorelbeke K, Vauterin S, Deckmyn H. Structural determinants within platelet glycoprotein Ibalpha involved in its binding to von Willebrand factor. Platelets 2000;11(7):373–8.
[48] Wang YM, Gao HY, Shi C, Erhardt PW, Pavlovsky A, Soloviev DA, et al. Leukocyte integrin Mac-1 regulates thrombosis via interaction with platelet GPIbα. Nat Commun 2017;8:15559.
[49] Wang Y, Li L, Zhao W, Dou Y, An H, Tao H, et al. Targeted therapy of atherosclerosis by a broad-spectrum reactive oxygen species scavenging nanoparticle with intrinsic anti-inflammatory activity. ACS Nano 2018;12(9):8943–60.
[50] Kong P, Cui ZY, Huang XF, Zhang DD, Guo RJ, Han M. Inflammation and atherosclerosis: signaling pathways and therapeutic intervention. Signal Transduct Target Ther 2022;7(1):131.
[51] Back M, AJr Yurdagul, Tabas I, Oorni K, Kovanen PT. Inflammation and its resolution in atherosclerosis: mediators and therapeutic opportunities. Nat Rev Cardiol 2019;16(7):389–406.
[52] Xiao ZC, Li Y, Xiong LY, Liao J, Gao YJ, Luo YC, et al. Recent Advances in anti-atherosclerosis and potential therapeutic targets for nanomaterial-derived drug formulations. Adv Sci (Weinh) 2023;10(29):e2302918.
[53] Wang D, Yang Y, Lei Y, Tzvetkov NT, Liu X, Yeung AWK, et al. Targeting foam cell formation in atherosclerosis: therapeutic potential of natural products. Pharmacol Rev 2019;71(4):596–670.
[54] Patel KM, Strong A, Tohyama J, Jin X, Morales CR, Billheimer J, et al. Macrophage sortilin promotes LDL uptake, foam cell formation, and atherosclerosis. Circ. Res. 2015;116(5):789–96.
[55] Moore KJ, Tabas I. Macrophages in the pathogenesis of atherosclerosis. Cell 2011;145(3):341–55.
[56] Irene FR. Macropinocytosis promotes foam cell formation and atherosclerosis. Nat Rev Cardiol 2022;19(12):781.
[57] Lin HP, Singla B, Ahn W, Ghoshal P, Blahove M, Cherian-Shaw M, et al. Receptor-independent fluid-phase macropinocytosis promotes arterial foam cell formation and atherosclerosis. Sci Transl Med 2022;14(663):eadd2376.